Structural study of nickelate based heterostructures

Lucia Varbaro ✉ iD ; Bernat Mundet iD ; Subhadeep Bandyopadhyay iD ; Claribel Domínguez;
Jennifer Fowlie iD ; Lukas Korosec ; Chih-Ying Hsu iD ; Duncan T. L. Alexander iD ; Philippe Ghosez iD ;
Jean-Marc Triscone iD

Check for updates

CrossMark

View Online

Export Citation

AIP Publishing

Structural study of nickelate based heterostructures

View Online   Export Citation   CrossMark

Lucia Varbaro,[1,a]   Bernat Mundet,[1,2]   Subhadeep Bandyopadhyay,[3]   Claribel Domínguez,[1] Jennifer Fowlie,[4]   Lukas Korosec,[1]   Chih-Ying Hsu,[1,2]   Duncan T. L. Alexander,[2]   Philippe Ghosez,[3] and Jean-Marc Triscone[1]

AFFILIATIONS

[1] DQMP, University of Geneva, Geneva, Switzerland
[2] Electron Spectrometry and Microscopy Laboratory (LSME), Institute of Physics (IPHYS), Ecole Polytechnique Fédérale de Lausanne (EPFL), Lausanne, Switzerland
[3] CESAM Research Unit, Université de Liège, Liège, Belgium
[4] Department of Applied Physics, Stanford University, Stanford, California 94305, USA

[a] Author to whom correspondence should be addressed: lucia.varbaro@unige.ch

ABSTRACT

Heterostructures consisting of $SmNiO_3$ and $NdNiO_3$ alternating layers with additional $LaAlO_3$ spacer layers were grown and fully characterized by means of x-ray diffraction, atomic force microscopy, and scanning transmission electron microscopy. A change in the orientation of the orthorhombic long-axis of the nickelate layers is observed when a single unit cell of $LaAlO_3$ is inserted between $SmNiO_3$ and $NdNiO_3$, in agreement with density functional theory calculations. At the same time, the structure of the ultra-thin rhombohedral $LaAlO_3$ layers is affected by their proximity to orthorhombic nickelate layers, with both scanning transmission electron microscopy studies and density functional theory calculations revealing a weak antipolar motion of the La-cation in the $LaAlO_3$ layers that is not present in the bulk rhombohedral structure of this compound.

I. INTRODUCTION

Transition metal oxide compounds,[1] and more specifically, transition metal perovskite oxides with the chemical formula ABO_3,[2] represent a vast playground for material engineering. This is mainly due to the plethora of physical properties they display, which depend on the choice made for the A and B cations.

Among them, metal-to-insulator transition (MIT) compounds such as rare earth nickelates ($RENiO_3$) have been deeply studied for understanding both their M–I transition[3,4] and complex magnetic state[5,6] and for their potential applications in novel devices.[7] The tunability of their MIT temperature also motivated the realization and study of interesting functional heterostructures made of nickelates or combinations of nickelates with other perovskites.[7]

As mentioned, nickelates are well known for their MIT, which occurs at a specific temperature (T_{MI}), ranging from 600 to 0 K

depending on the chosen rare earth cation. This value depends on the degree of distortion of the structure, which is in turn determined by the size of the A-cation. Along with this electronic transition, nickelates display a structural transition from a high temperature orthorhombic symmetry (rotation pattern $a^-a^-c^+$ in the Glazer notation) to a low T monoclinic structure with a similar tilt pattern. In the low T structure, a breathing distortion is observed with alternating large oxygen octahedra (long bond) and smaller ones (short bond).[7] Due to its twofold nature, the transition can be described by two different order parameters. First, an electronic one, ΔN, which describes the difference in occupation number between the Ni 3d e_g orbitals of two inequivalent nickel sites (Ni-1 and Ni-2 located at the center of the long bond and short bond oxygen octahedra, respectively), is characteristic of the insulating ground state phase. Second, Q is a structural one, which is defined as the size difference between the large and small oxygen octahedra.[8–11]

In previous work (Refs. 12 and 13), superlattices made of two different nickelate compounds (respectively, $NdNiO_3$ and $SmNiO_3$) were studied in order to investigate the length scale over which a coexistence between metallic and insulating phases can be established. More recently, in Ref. 11, insulating $LaAlO_3$ spacer layers were introduced between the nickelate layers to better understand the interfacial behavior of the order parameters controlling the transition (ΔN and Q). These more complex heterostructures were made of repeating stacks of (m $NdNiO_3$/d $LaAlO_3$/m $SmNiO_3$/d $LaAlO_3$)—m and d being, respectively, the thickness in unit cells of the nickelate layers and $LaAlO_3$ spacer layers. These structures were grown on top of (001) pseudo-cubic oriented $LaAlO_3$ substrates and characterized.

In Ref. 11, the transport properties (resistivity vs temperature and Hall effect measurements) of these heterostructures were studied in detail. The main findings of this previous study can be summarized as follows: For $d = 0$ (no $LaAlO_3$, $SmNiO_3$/$NdNiO_3$ superlattices), below a critical thickness of the nickelate layers, the system displays a single MIT temperature, as expected from the study realized in Ref. 12. However, for all the samples with d $LaAlO_3$ not equal to zero, $d = 1, 2, 3,$ and 4, the two layers behave independently—and the system displays two different transitions in the resistivity vs temperature curves—indicative of a decoupling of the two layers.

Here, we investigate in detail the structure of these transition metal oxide superlattices through the quantitative analysis of scanning transmission electron microscopy (STEM) data, combined with density functional theory (DFT) calculations. Remarkably, we observe a reorientation of the orthorhombic long axis of the nickelates, whose rotation pattern in Glazer notation is $a^-a^-c^+$ for the $Pbnm$ structure (c^+ denoting the so-called long axis, along which the oxygen octahedra rotate in phase). While for nickelate films and superlattices grown on $LaAlO_3$ substrates, the long-axis is always found to be pointing in-plane (parallel to the substrate interface)—the configuration minimizing macroscopic strain[14]—the presence of the spacer layers induces a flip of its direction, which is now found to be pointing out-of-plane across most of the heterostructure. Surprisingly, we also find that the $LaAlO_3$ spacer layer, rhombohedral in bulk with an $a^-a^-a^-$ tilt pattern, develops an antipolar motion of the A-site cations below some critical thickness. These experimental findings are corroborated by DFT calculations.

II. EXPERIMENTAL SECTION

Figure 1 displays a characterization of an example of the m $NdNiO_3$/d $LaAlO_3$/m $SmNiO_3$/d $LaAlO_3$ structures under study. As can be seen from both the high-angle annular dark field (HAADF) STEM images in Figs. 1(a) and 1(b) and the electron energy-loss spectroscopy (EELS) compositional map in Fig. 1(d), the sample displays high crystalline quality and a low degree of chemical intermixing. The structural quality is confirmed by the typical x-ray diffraction θ–2θ scans shown in Fig. 1(c). It is important to note that all the samples investigated here grow coherently on $LaAlO_3$, i.e., without dislocations or relaxation of the grown structure.[11]

We now leverage STEM imaging to obtain insights into the structural nature of the heterostructures. First, we apply a technique based on the adapted geometrical phase analysis (GPA) of aberration-corrected HAADF STEM images that was developed in Ref. 14 to simultaneously visualize different $Pbnm$ domains within the same image and map the crystallographic orientation across the studied superlattices. As mentioned before, the rotation pattern of the $Pbnm$ structure is $a^-a^-c^+$. These three rotations couple to an X_5^- antipolar mode (AM), which corresponds to A-site cation displacements along the $[1,0,0]_o$ and $[\bar{1},0,0]_o$ directions, the previously mentioned antipolar motion. Using the adapted GPA, this antipolar motion is rendered as lines of positive and negative contrasts in a "shear-strain" map. The operating principle behind this is the choice of specific reciprocal-space virtual aperture settings for the strain calculation by the GPA algorithm. These virtual apertures are selected in such a way as to include the half-order peaks associated with the X_5^- mode. In itself, this mode constitutes a signature of the orthorhombic structure and is not present in the rhombohedral phase.

Figure 2(a) shows a sketch of a 6 $NdNiO_3$/6 $SmNiO_3$ superlattice without $LaAlO_3$ spacer layers. Figure 2(b) displays a HAADF image of the superlattice, with accompanying adapted-GPA mapping of A-site antipolar motion on the right. The vertical stripes of the latter colormap correspond to vertical alternating displacements of the A-cations, henceforth determining that the orthorhombic long-axis lies in-plane as indicated in the figure. The XRD rocking curves (ω scans) displayed in Fig. 2(c) show the presence and absence of $(0, -\frac{1}{2}, 1)_{pc}$ and $(0, -1, \frac{1}{2})_{pc}$, respectively. These half order peaks arise because of the aforementioned X_5^- distortion, which doubles the unit cell along one pseudo-cubic axis. Since only the former peak is present, this confirms the in-plane orientation of the orthorhombic long axis found using the GPA analysis. The same analyses are performed on a 6 $NdNiO_3$/2 $LaAlO_3$/6 $SmNiO_3$/2 $LaAlO_3$ superlattice, as shown in Figs. 2(d)–2(f). The adapted GPA colormap in (e) reveals horizontal stripes, indicating that the orthorhombic long-axis of the nickelate layers now points out-of-plane. This structural orientation is confirmed by XRD in panel (f). Remarkably, therefore, the insertion of ultra-thin $LaAlO_3$ spacers between the $RENiO_3$ layers produces a flip of the long-axis orientation, from in-plane to out-of-plane.

In orthorhombic films grown on substrates having, such as the $LaAlO_3$ used here, cubic cation sublattices,[14] the strain state of the film is a common determinant of its orientation. Here, the strain state of the nickelate layers is not modified by the insertion of the $LaAlO_3$ layers.[11] Therefore, the observed flip in orthorhombic long-axis orientation may seem surprising. Our DFT calculations do, in fact, confirm that the long-axis in plane is the minimum energy configuration without $LaAlO_3$ layers, whereas the energy is minimized with a long-axis out-of plane when introducing the spacer layers (see the supplementary material section, Fig. S1). Phenomenologically, a possible explanation for this change in the long-axis orientation derives from the connectivity of oxygen octahedra rotations (OORs). While $LaAlO_3$ has out-of-phase OOR along all three axes, the long-axis of the orthorhombic nickelate structure has in-phase OOR. If this long-axis points in-plane (as favored by strain state alone), it will create a mismatch with the out-of-phase OOR of the $LaAlO_3$ layers sandwiching it on either side. It appears that the energetic cost of creating interfaces that couple these mismatched OORs is sufficient to drive the nickelate layers to point their long-axis out-of-plane. This way, the nickelate layers present only out-of-phase OOR
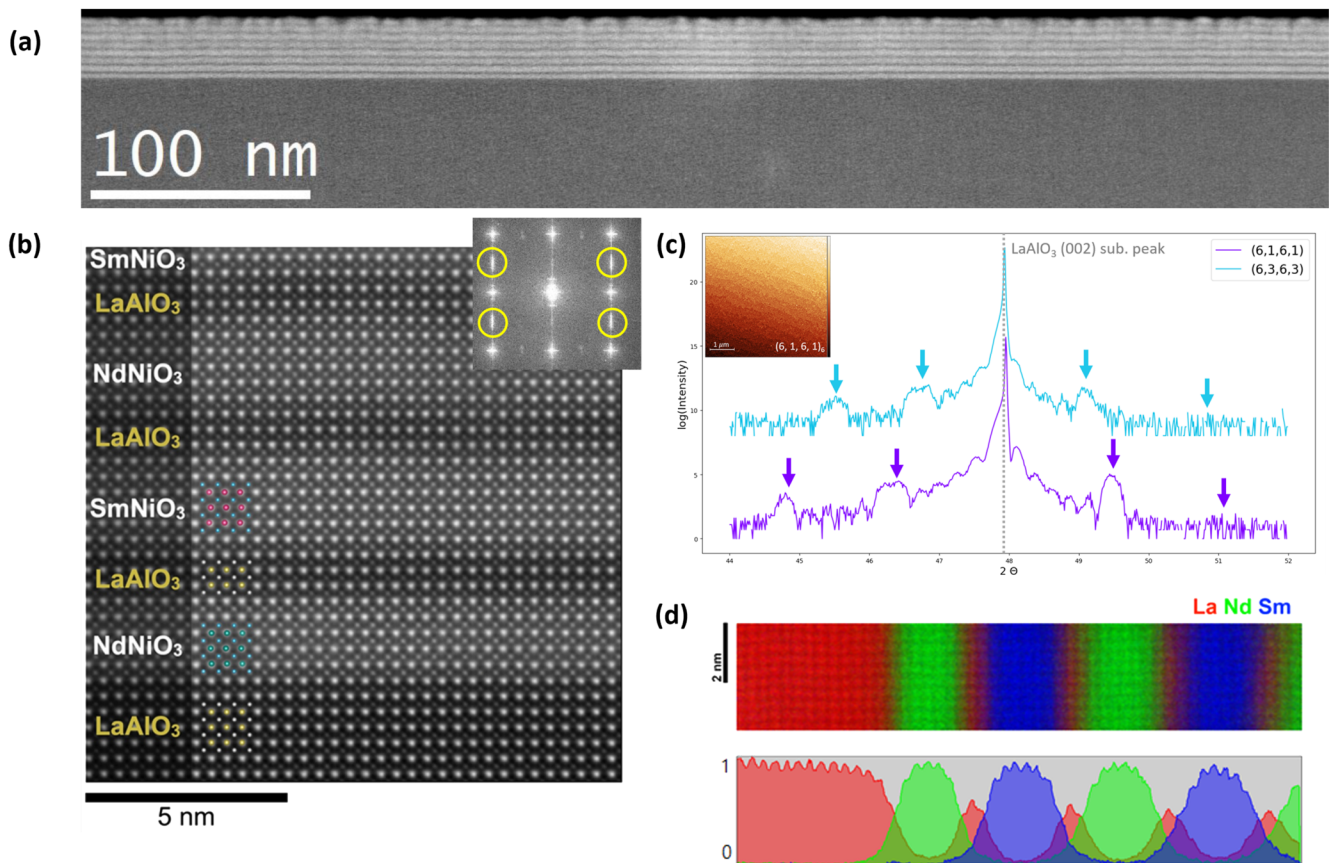
FIG. 1. (a) Low magnification STEM image of a 4 NdNiO$_3$/2 LaAlO$_3$/4 SmNiO$_3$/2 LaAlO$_3$ superlattice reveals a very homogeneous heterostructure without secondary phases. (b) High magnification STEM image of the same superlattice, in which a sketch of the cation positions has been superimposed for clarity. The inset shows the Fourier transform of the high resolution image, displaying the half order reflections (indicated by the yellow circles) due to the orthorhombic unit cell symmetry, i.e., doubling of the unit cell. (c) X-ray diffraction (XRD) θ–2θ scan around the (002) substrate reflection of a (6, 1, 6, 1) and (6, 3, 6, 3) superlattice, respectively in purple and light blue. The arrows indicate the satellite peaks of the superlattices, while the gray dashed line marks the (002) substrate reflection. The inset shows the surface of the sample, obtained through atomic force microscopy (AFM) measurements, which shows a step-terrace structure resembling that of the substrate. (d) Compositional map of the superlattice along the sample growth direction showing the spatial distribution of each element and the integrated chemical profile, pointing to a low degree of intermixing and relatively sharp interfaces between the layers.

in the substrate plane, which then matches better the out-of-phase OOR of the sandwiching LaAlO$_3$ layers. Evidently, the interfacial energy reduction from avoiding OOR pattern mismatch is sufficient to compensate for the increase in macroscopic strain energy.

For samples with thicker LaAlO$_3$ spacer layers (at least 4 u.c.), it was shown that the interface roughness increases.[11] At the same time, we no longer observe a uniform flip of the orthorhombic long axis (see the supplementary material, section Fig. S2). This observation is likely due to the small difference in energy between the two configurations (in-plane or out-of-plane long-axis), which was found to be 2 meV/5 atom f.u. in our DFT calculations. The increase in interfacial disorder in these samples, tied to a decrease in the density of interfaces, probably affects the OOR coupling, making the two configuration possibilities very close in energy, such that neither of them predominates.

An open question is why this mechanism does not occur for single nickelate films or heterostructures (without LaAlO$_3$ spacer layers) since they are grown on a rhombohedral LaAlO$_3$ substrate. A possible explanation is linked to the fact that, in these new super-lattices, we have thin nickelate layers both grown on LaAlO$_3$ and capped with LaAlO$_3$. The OOR coupling thus occurs on both sides of each nickelate layer, giving a relatively strong energetic influence. In comparison, for structures without spacer layers, the OOR coupling occurs only at the single substrate/film interface; it appears insufficient to induce a long axis reorientation away from that favored by the macroscopic strain state, given the low energy difference between the two configurations found in DFT calculations as discussed above.

Since this difference in energy is small, there should also be in superlattices with LaAlO$_3$ spacer layers a critical thickness of
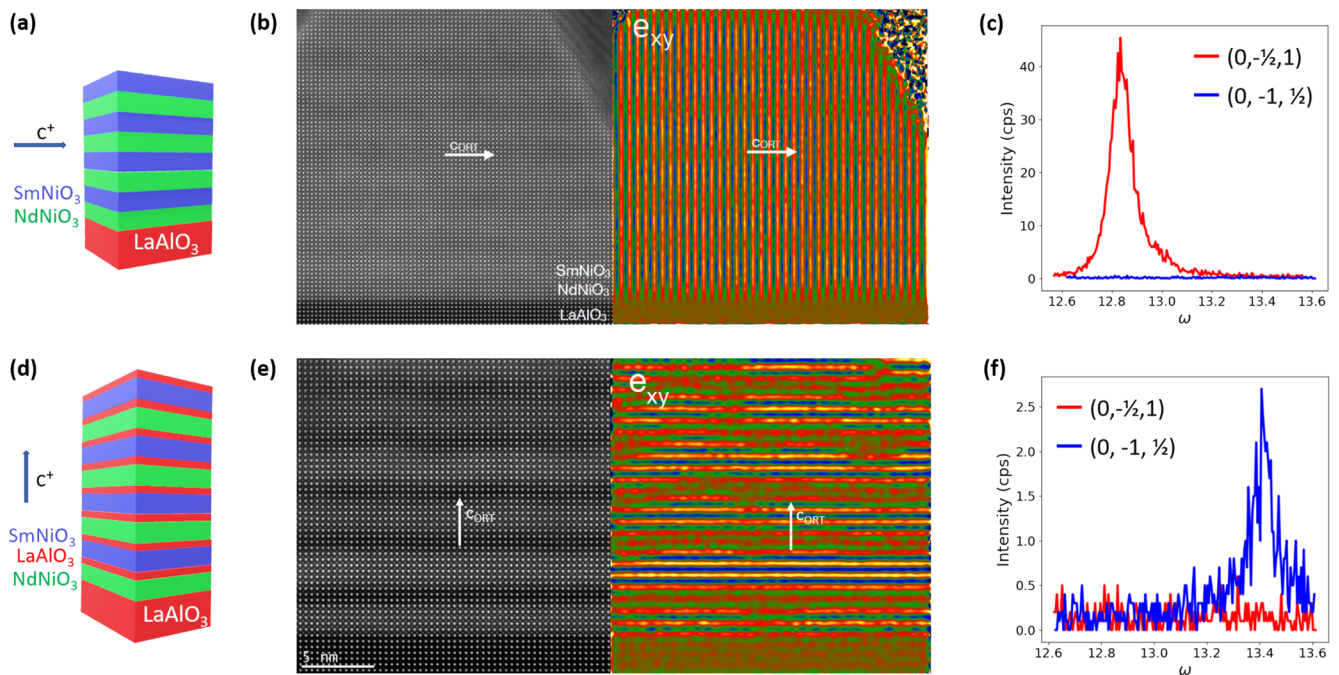
FIG. 2. (a) Sketch of a $NdNiO_3/SmNiO_3$ superlattice without a $LaAlO_3$ spacer. (b) High magnification HAADF STEM image of a 6 $NdNiO_3$/6 $SmNiO_3$ superlattice and corresponding adapted-GPA indicating a vertical antipolar motion of the A-cations, which in turn indicates that the orthorhombic long axis lies in the plane of the substrate. (c) X-ray diffraction ω scan around the half-order reflection of the superlattice confirms the crystallographic orientation identified by STEM. (d)–(f) Analogous analysis performed on a 6 $NdNiO_3$/2 $LaAlO_3$/6 $SmNiO_3$/2 $LaAlO_3$ superlattice, displays the opposite behavior, i.e., the orthorhombic long axis points in the out-of-plane direction.

the nickelate individual layers, above which the macroscopic strain energy (that increases with the thickness of the nickelate layer) will win against the interfacial cost linked to oxygen octahedra coupling, which instead does not depend on thickness. This should lead to a long axis in-plane reorientation.

Having studied the nickelate layers, we now turn our attention to the structure of the $LaAlO_3$ spacer layers in the superlattices as a function of their thickness. First, we note that, in bulk, $LaAlO_3$ is a large bandgap insulator, which crystallizes in a rhombohedral $R\bar{3}c$ structure with, as mentioned above, a Glazer tilt rotation pattern $a^-a^-a^-$. This corresponds to out-of-phase rotations of the AlO_6 octahedra along the three pseudocubic axes with identical rotation amplitudes. Phonon spectra calculations using a cubic structure of $LaAlO_3$[15] show that the system displays three unstable modes at the high symmetry R point, which condense in the 0 K calculations and lead to the rhombohedral ground state structure. Furthermore, phonon spectra for cubic $LaAlO_3$ do not reveal any other unstable modes at any other high symmetry points. The system is thus not close to in-phase octahedral or polar distortion instabilities. DFT calculations of the $LaAlO_3$ structure show, in particular, that it is very costly to try enforcing an in-phase rotation in one of the directions. It is also worth mentioning that the $Imma$ ($I4/mcm$) phase of the $LaAlO_3$—with Glazer notation $a^-a^-c^0$ ($a^-b^0b^0$)—can be achieved by applying tensile (compressive) strain as this phase is energetically very close to the ground state $R\bar{3}c$ phase. The calculations thus show that, although one or two of the out-of-phase rotations can be

suppressed in $LaAlO_3$, it is very challenging to impose the in-phase rotations. Clearly, this is consistent with the observed imposition of an out-of-plane orthorhombic long-axis on the nickelate layers, such that out-of-phase OOR can be maintained in the $LaAlO_3$ spacer layers.

Despite this, an unexpected distortion is observed in the thinnest $LaAlO_3$ spacer layers. Figure 3(a) shows a section of a STEM-HAADF image of one superlattice of the series, specifically (6,3,6,3). Figure 3(b) presents the adapted GPA of this image section; it displays horizontal stripes, consistent with the out-of-plane orthorhombic long axis direction of the nickelate layers. From the full high-resolution image, which measures 54 pseudocubic unit cells in width, the average displacement of the A-site cation has been extracted for each atomic layer, as displayed in Fig. 3(c). Plotting the absolute value of the AM in panel (d) reveals two aspects. First, the AM distortions in the nickelate slabs are reduced when in proximity to the $LaAlO_3$ layers. Second, surprisingly, the AM is not completely suppressed in the nominally rhombohedral $LaAlO_3$ thin layers (for which no antipolar motion is expected) but rather propagates across them.

Analogous analyses of a (6,2,6,2) superlattice show very similar behavior (Fig. S3 of the supplementary material section). It is important to note that there is a certain imprecision in this finding because of the finite miscut angle of the substrate and the film deposition method, meaning that the atomic column projections observed by STEM at any superlattice interface can contain a mix-
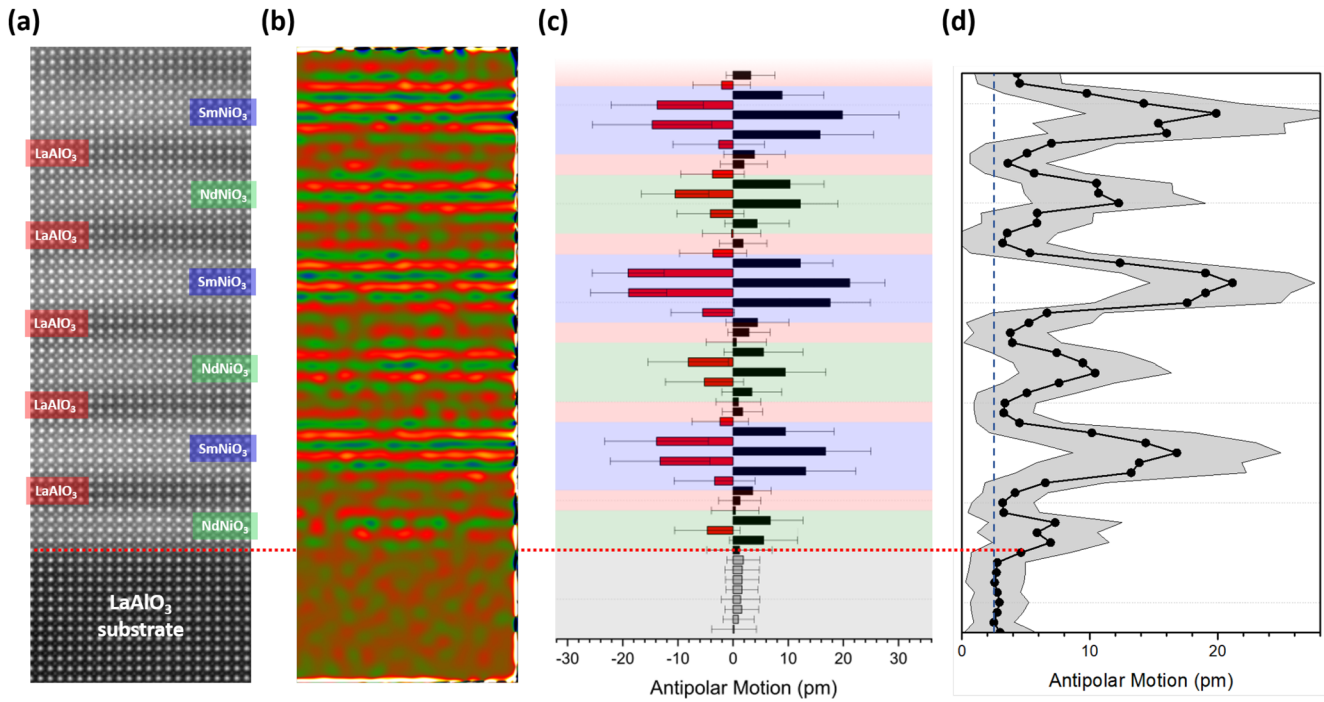
FIG. 3. (a) STEM-HAADF image of a (6,3,6,3) superlattice and (b) adapted GPA e_{xy} map displaying the antipolar motion of the A-cations along the in-plane direction (as explained previously). From the full image, the averaged displacements of the A-cations are extracted in plot (c). Note that the AM is larger in the $SmNiO_3$ layers (blue) than in the $NdNiO_3$ layers (green), as expected. The AM amplitude is reduced in the nickelate layers of the A-planes in proximity to $LaAlO_3$. Importantly, while reduced, the AM is not zero in the $LaAlO_3$ spacer layers, as can also be inferred by the faint but still present horizontal stripes in the GPA map locations corresponding to the $LaAlO_3$ layers. The red dotted line indicates the interfacial atomic plane between the $LaAlO_3$ substrate and the first $NdNiO_3$ layer. Panel (d) shows the absolute values of the AM. When plotting such an absolute value, noise in the measurement inherently leads to a non-zero value, even if the structure contains zero AM. Therefore, the measured value of the $LaAlO_3$ substrate (containing zero AM in its rhombohedral structure) can be taken as a proxy for zero AM, as indicated by the blue dashed vertical line. It is seen that, within the $LaAlO_3$ spacer layers, the magnitude of AM does not decrease to this reference "zero" value.

ture of both compounds on either side, resulting in a 1 u.c. error bar on the thickness of the layers. Nevertheless, when inspecting superlattices with thicker $LaAlO_3$ layers such as the (6,4,6,4) sample, which, as previously described, have lower structural quality and decreased symmetry-imposition of orthorhombic orientation on the nickelate layers, no analogous AM is observed in the $LaAlO_3$ spacer layers, thereby indicating that the observation of AM in the thinnest $LaAlO_3$ layers is not an artifact.

Given that the orthorhombic long-axis (having in-phase OOR) of the nickelate layers is out-of-plane, it can be questioned why $LaAlO_3$ develops an antipolar motion. The coupling of rotations is typically weak along an out-of-plane axis.[16–19] Combined with in-phase OOR being highly unfavorable in $LaAlO_3$, it is, therefore, unlikely that the thinnest $LaAlO_3$ spacer layers take on the OOR pattern of an orthorhombic compound, as typically associated with an A-cation AM. Alternatively, a possible reason comes from the A-cations themselves. At interfaces, the La cations of the $LaAlO_3$ spacer layers experience the potential landscape of the Nd and Sm cations of the adjacent layers. Since the latter atoms are displaced in-plane by their AM, their interaction with the La "lattice" may induce an antipolar motion in the

$LaAlO_3$ layers. This may explain the surprising change in the $LaAlO_3$ structure, which, in these superlattices, is no longer "purely" rhombohedral.

To better understand the structure of the thin $LaAlO_3$ layers and, in particular, to confirm the observation of antipolar motion in them, DFT calculations are performed for different structures. In these simulations, the orthorhombic long axis of the nickelate layers is imposed to point in the out-of-plane direction, as observed experimentally in the superlattices containing $LaAlO_3$ studied here. This configuration is also the one that minimizes the energy in the DFT calculations (Fig. S1). Figures 4(c) and 4(d) display the results of DFT calculations performed on a (3,1,3,1) and (3,2,3,2) $NdNiO_3/LaAlO_3/SmNiO_3/LaAlO_3$ superlattices, while Figs. 4(a) and 4(b) constitute a study on simpler structures, respectively, four layers of strained $NdNiO_3$ and 3–1 layers of $NdNiO_3$-$LaAlO_3$. From the latter structure, it is clear that the proximity to $LaAlO_3$ influences both the OOR and the AM pattern of the A-cation in the nickelate layer. Without the $LaAlO_3$ spacer, Fig. 4(a), the out-of-phase OOR angles ϕ_a/ϕ_b display an amplitude of 7.66°, while an amplitude of the in-phase rotations ϕ_c of 6.99° is obtained, which differs from bulk $NdNiO_3$ due to the epitaxial strain (see the supplementary material
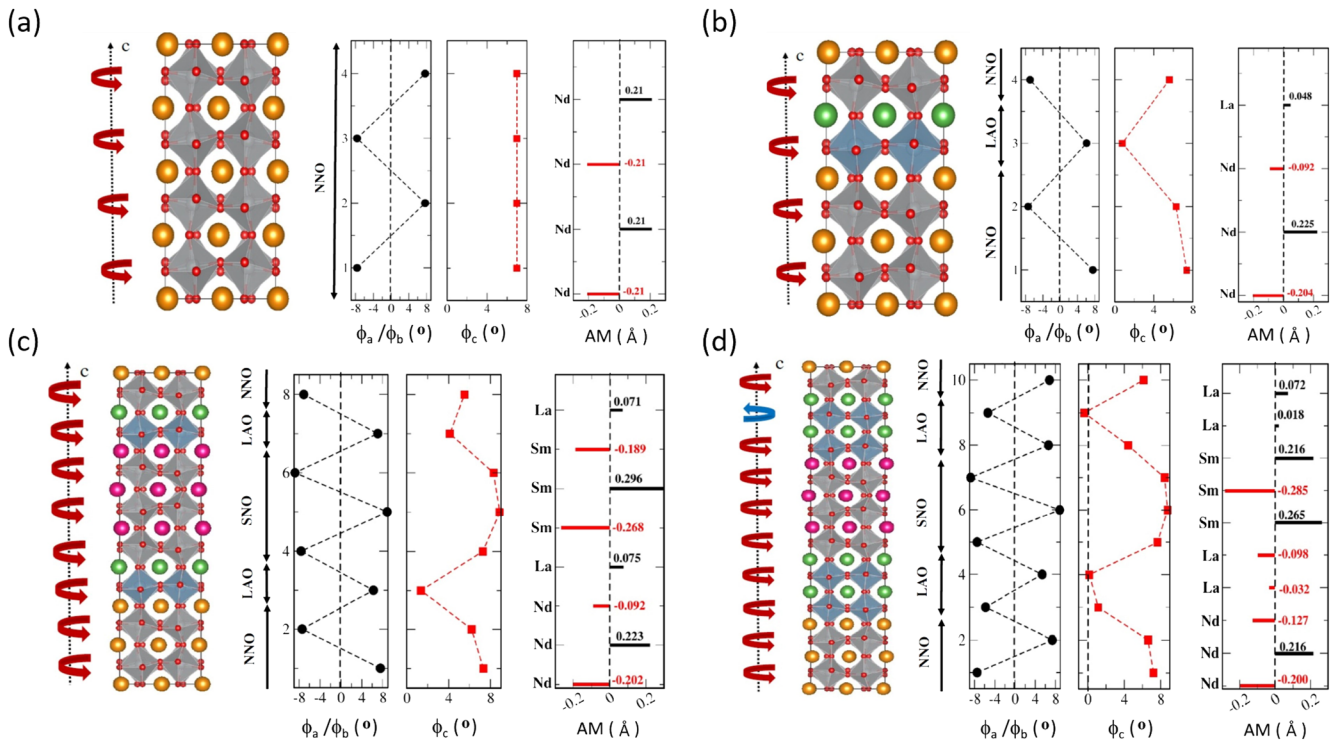
FIG. 4. DFT calculations performed on different relaxed nickelate-based structures—with the orthorhombic long axis pointing in the out-of-plane direction in the nickelate layers—displaying the amplitude of the out-of phase (ϕ_a/ϕ_b) and in-phase (ϕ_c) rotations and the relative antipolar motion of the A cation, respectively, for (a) pure NdNiO$_3$ (NNO), for which the rotation amplitudes differ from the bulk values due to the compressive strain and the AM cancels out perfectly; (b) a heterostructure consisting of the repetition of 3 u.c. of NdNiO$_3$ and 1 u.c. of LaAlO$_3$ (LAO), in which the latter both induces a reduction in the in-phase rotation amplitudes and leads to a modification in the A-cation pattern in both the NdNiO$_3$ and LaAlO$_3$; (c) a (3,1,3,1) NdNiO$_3$, LaAlO$_3$, SmNiO$_3$ (SNO) superlattice, in which a suppression of ϕ_c at the interfaces between the nickelate layers and LaAlO$_3$ is also observed (an effect which is more pronounced at the LaAlO$_3$-SmNiO$_3$ interface), again linked to a non-zero AM in the LaAlO$_3$ layers; and (d) a (3,2,3,2) NdNiO$_3$, LaAlO$_3$, SmNiO$_3$ heterostructure, in which additionally, the A-cations do not follow a uniform pattern of displacements, but adopt a configuration that would seemingly produce a net polarization.

section, Fig. S4). Furthermore, the antipolar motion, shown in Å in the last column in Fig. 4(a), perfectly cancels out in consecutive Nd layers. Upon the introduction of 1 unit cell of LaAlO$_3$ [Fig. 4(b)], the values of the OOR in the c-direction for NiO$_6$ octahedra are modified. Tied to this, the A-cation displacements are modified; not only do the La cations adopt a non-zero displacement, giving a first hint of the experimental observation in the more complex superlattices, but the Nd cations take non-uniform absolute displacement values.

Turning to Fig. 4(c) and the results for the optimized structure of a (3,1,3,1) superlattice, one can observe that the suppression of the LaAlO$_3$ in-phase rotations (ϕ_c) is larger at the NdNiO$_3$ interfaces than at the SmNiO$_3$ ones. This may be the consequence of the smaller bulk rotation amplitudes of NdNiO$_3$ as compared to the ones of SmNiO$_3$. One also notices a strongly reduced in-phase rotation close to the La plane, in line with the difficulty noted earlier in developing in-phase rotations in LaAlO$_3$. In addition, observed is that the antipolar motion of the La-cations mostly follows the alternate motion of the Sm and Nd layers, a result

consistent with the experimental observations described above. Together, this leads to a non-cancellation of the net A-site cation displacements.

Figure 4(d) shows the results for an energy-minimized structure in which the number of LaAlO$_3$ layers inside the heterostructure is increased to 2 u.c. but the thickness of the ReNiO$_3$ layers remains 3 u.c. Such a (3,2,3,2) replicates more closely the experimentally measured samples. Here, we see a very large suppression of the rotation amplitude of the oxygen octahedra in between the two AlO planes. For the octahedra sandwiched between AlO and NdO, the rotations are non-vanishing but are again more strongly reduced than the ones of the octahedra in between AlO and SmO planes. Nevertheless, LaAlO$_3$ seems to partly recover its bulk-like out-of-phase rotation in all directions. However, that depends strongly on the cation environment and again leads to a non-uniform pattern in the A-cation motion. This resulting complex pattern should introduce a net polarization, which in turn could provide a path toward producing in-plane improper ferroelectricity.

III. CONCLUSION

In conclusion, high crystalline quality heterostructures made of $SmNiO_3$ and $NdNiO_3$ with $LaAlO_3$ spacer layers were grown and characterized in-depth by means of XRD, AFM, and STEM. The structural study presented here reveals that the insertion of the $LaAlO_3$ layers has a strong effect on the orientation of the orthorhombic long-axis of the nickelate layers. While the long-axis is always in-plane when growing single compound films and superlattices made only of nickelates on $LaAlO_3$ substrates (as expected from the macroscopic strain state), when 2 or 3 u.c. $LaAlO_3$ spacer layers are inserted between the nickelate layers, the orthorhombic long-axis flips out-of-plane. This result is in agreement with DFT calculations, which further reflect this phenomenon when just a single u.c. of $LaAlO_3$ is inserted as a spacer layer. The observed change in the orientation of the long-axis can be explained by considering OOR coupling at the multiple interfaces between materials displaying different crystal structures in their bulk-like form. This study illustrates how the lattice orientation in *Pbnm* systems can be manipulated by combining the *Pbnm* layers ($a^-a^-c^+$) with rhombohedral $R\bar{3}c$ ones, which instead display a bulk $a^-a^-a^-$ rotation pattern. Such manipulations might be important for controlling the electronic properties of some transition metal oxides. For instance, magnetism in $LaMnO_3/GdScO_3$ was found to depend on the orientation of the long-axis.[20] Between experiments and simulations, we also find that the crystallographic structure of ultra-thin $LaAlO_3$ spacer layers sandwiched between nickelate layers changes; they both develop an antipolar motion and display markedly reduced out-of-plane rotation amplitudes. This very unusual finding can possibly be explained by the electrostatic interaction between the A cations at interfaces. Since it is well known that rather small changes in the crystallographic structure of a correlated material can drastically modify its displayed properties, our findings provide a possible path to engineering functional properties by controlling the long axis orientation and antipolar motion.

SUPPLEMENTARY MATERIAL

The supplementary material contains the following: 1. Additional DFT calculations for a (3,1,3,1) superlattice. 2. STEM image and GP analysis of a (6,4,6,4) superlattice. 3. High resolution STEM image and antipolar motion pattern relative to (6,2,6,2) SL. 4. Simulated amplitude of the octahedral rotations in bulk $SmNiO_3$, $NdNiO_3$, and $LaAlO_3$.

ACKNOWLEDGMENTS

AUTHOR DECLARATIONS

Conflict of Interest

The authors have no conflicts to disclose.

Author Contributions

Lucia Varbaro: Data curation (equal); Investigation (equal); Writing – original draft (equal). **Bernat Mundet**: Data curation (equal); Formal analysis (equal); Investigation (equal); Methodology (equal); Writing – review & editing (equal). **Subhadeep Bandyopadhyay**: Data curation (equal); Formal analysis (equal); Writing – review & editing (equal). **Claribel Domínguez**: Conceptualization (equal); Writing – review & editing (equal). **Jennifer Fowlie**: Conceptualization (equal); Supervision (equal); Writing – review & editing (equal). **Lukas Korosec**: Conceptualization (equal); Data curation (equal); Writing – review & editing (equal). **Chih-Ying Hsu**: Data curation (equal); Formal analysis (equal). **Duncan T. L. Alexander**: Data curation (equal); Formal analysis (equal); Investigation (equal); Methodology (equal); Writing – review & editing (equal). **Philippe Ghosez**: Conceptualization (equal); Supervision (equal); Writing – review & editing (equal). **Jean-Marc Triscone**: Conceptualization (equal); Investigation (equal); Project administration (equal); Supervision (equal); Writing – review & editing (equal).

DATA AVAILABILITY

The data that support the findings of this study are available at Yareta repository upon reasonable request.

REFERENCES

[1] D. I. Khomskii, *Transition Metal Compounds* (Cambridge University Press, Cambridge, 2014).

[2] J. B. Goodenough, "Electronic and ionic transport properties and other physical aspects of perovskites," Rep. Prog. Phys. **67**(11), 1915 (2004).

[3] M. L. Medarde, "Structural, magnetic and electronic properties of $RNiO_3$ perovskites (R = rare earth)," J. Phys.: Condens. Matter **9**(8), 1679–1707 (1997).

[4] G. Catalan, "Progress in perovskite nickelate research," Phase Transitions **81**(7–8), 729–749 (2008).

[5] M. T. Fernández-Díaz, J. A. Alonso, M. J. Martínez-Lope, M. T. Casais, and J. L. García-Muñoz, "Magnetic structure of the $HoNiO_3$ perovskite," Phys. Rev. B **64**(14), 144417 (2001).

[6] J. L. García-Muñoz, J. Rodríguez-Carvajal, and P. Lacorre, "Neutron-diffraction study of the magnetic ordering in the insulating regime of the perovskites $RNiO_3$ (R = Pr and Nd)," Phys. Rev. B **50**(2), 978–992 (1994).

[7] S. Catalano, M. Gibert, J. Fowlie, J. Íñiguez, J.-M. Triscone, and J. Kreisel, "Rare-earth nickelates $RNiO_3$: Thin films and heterostructures," Rep. Prog. Phys. **81**(4), 046501 (2018).

[8] O. E. Peil, A. Hampel, C. Ederer, and A. Georges, "Mechanism and control parameters of the coupled structural and metal-insulator transition in nickelates," Phys. Rev. B **99**(24), 245127 (2019).

[9] A. B. Georgescu and A. J. Millis, "Quantifying the role of the lattice in metal–insulator phase transitions," Commun. Phys. **5**(1), 135 (2022).

[10] A. B. Georgescu, O. E. Peil, A. S. Disa, A. Georges, and A. J. Millis, "Disentangling lattice and electronic contributions to the metal–insulator transition from bulk vs. layer confined $RNiO_3$," Proc. Natl. Acad. Sci. U. S. A. **116**(29), 14434–14439 (2019).

[11] L. Varbaro, B. Mundet, C. Domínguez, J. Fowlie, A. B. Georgescu, L. Korosec, D. T. Alexander, J. Triscone, and J.-M. Triscone, "Electronic coupling of metal-to-insulator transitions in nickelate-based heterostructures," Adv. Electron. Mater. **9**(5), 2201291 (2023).

[12] C. Domínguez, A. B. Georgescu, B. Mundet, Y. Zhang, J. Fowlie, A. Mercy, A. Waelchli, S. Catalano, D. T. L. Alexander, P. Ghosez, A. Georges, A. J. Millis, M. Gibert, J. M. Triscone, and J.-M. Triscone, "Length scales of interfacial coupling

between metal and insulator phases in oxides," Nat. Mater. **19**(11), 1182–1187 (2020).

[13] B. Mundet, C. Domínguez, J. Fowlie, M. Gibert, J.-M. Triscone, D. T. L. Alexander, and L. Alexander, "Near-atomic-scale mapping of electronic phases in rare earth nickelate superlattices," Nano Lett. **21**(6), 2436–2443 (2021).

[14] B. Mundet, M. Hadjimichael, J. Fowlie, L. Korosec, L. Varbaro, C. Dominguez, J.-M. Triscone, T. Duncan, and L. Alexander, "Mapping orthorhombic domains with geometrical phase analysis in rare-earth nickelate heterostructures," APL Mater. (to be published).

[15] R. Vali, "Phonons and heat capacity of LaAlO₃," Comput. Mater. Sci. **44**(2), 779–782 (2008).

[16] Z. Liao, M. Huijben, Z. Zhong, N. Gauquelin, S. Macke, R. J. Green, S. Van Aert, J. Verbeeck, G. Van Tendeloo, K. Held, G. A. Sawatzky, G. Koster, and G. Rijnders, "Controlled lateral anisotropy in correlated manganite heterostructures

[17] E. J. Moon, R. Colby, Q. Wang, E. Karapetrova, C. M. Schlepütz, M. R. Fitzsimmons, and S. J. May, "Spatial control of functional properties via octahedral modulations in complex oxide superlattices," Nat. Commun. **5**(1), 5710 (2014).

[18] J. M. Rondinelli, S. J. May, and J. W. Freeland, "Control of octahedral connectivity in perovskite oxide heterostructures: An emerging route to multifunctional materials discovery," MRS Bull. **37**(3), 261–270 (2012).

[19] J. M. Rondinelli and N. A. Spaldin, "Structure and properties of functional oxide thin films: Insights from electronic-structure calculations," Adv. Mater. **23**(30), 3363–3381 (2011).

[20] M. Schmitt, "Control of octahedral connectivity in perovskite oxide heterostructures: An emerging route to multifunctional materials discovery," Ph. D. thesis (Université de Liège, 2020).

by interface-engineered oxygen octahedral coupling," Nat. Mater. **15**(4), 425–431 (2016).